Case Studies in Thermal Engineering 54 (2024) 103993

Contents lists available at ScienceDirect

Case Studies in Thermal Engineering

journal homepage: www.elsevier.com/locate/csite

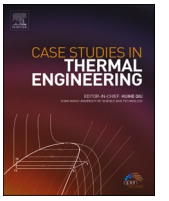

New pressure drop and heat transfer correlations for turbulent forced convection in internally channeled tube heat exchanger ducts

Abbas J.S. Al-Lami [a,b], Eugeny Y. Kenig [a,*]

[a] Paderborn University, Chair of Fluid Process Engineering, Paderborn, Germany
[b] University of Misan, Chair of Mechanical Engineering, Misan, Iraq

ARTICLE INFO

Handling Editor: Huihe Qiu

Keywords:
Internally channeled tubes
Heat exchanger
Friction factor
Nusselt number
Correlations

ABSTRACT

In our previous paper, a novel heat exchanger concept, the so-called internally channeled tube (ICT) was suggested, based on a tubular geometry fitted with specially designed curved channels along the tube length. The enhanced heat transfer in the ICT results from extended surface area between two contacting fluids. To facilitate industrial application, ICT design methods must be developed. This work provides new equations for thermo-hydraulic characterization of ICT under turbulent flow conditions. In particular, new friction factor and Nusselt number correlations are derived based on the validated CFD simulations performed over a wide range of Reynolds numbers and geometrical parameters.

Nomenclature

A	area, [m^2]
a,b,c,e,s	geometrical parameters of ICT ducts, [m]
c_p	specific heat, [J kg^{-1} K^{-1}]
D	diameter, [m]
d	tube diameter, [m]
f	friction factor, [−]
h_{avg}	average heat transfer coefficient, [W m^{-2} K^{-1}]
l	length of test section, [m]
$\dot{m}$	mass flowrate, [kg s^{-1}]
Nu	Nusselt number, [−]
P	perimeter, [m]
Pr	Prandtl number, [−]
q	heat flux, [W m^{-2}]
r	radius of the tube, [m]
Re_h	Reynolds number based on hydraulic diameter, [−]
T	temperature, [K]

* Corresponding author. Paderborn University, Chair of Fluid Process Engineering, Pohlweg 55, Paderborn, Germany.
E-mail address: eugeny.kenig@upb.de (E.Y. Kenig).

https://doi.org/10.1016/j.csite.2024.103993
Received 16 October 2023; Received in revised form 28 December 2023; Accepted 6 January 2024
Available online 7 January 2024

t	internal wall thickness, [m]
u	velocity, [m s^{-1}]
x,y,z	Cartesian coordinates, [m]

Greek symbols

Δp	pressure drop, [Pa]
λ	thermal conductivity, [W m^{-1} K^{-1}]
μ	dynamic viscosity, [Pa s]
ρ	density, [kg m^{-3}]
ν	kinematic viscosity, [m^2 s^{-1}]

Subscripts

b	bulk
cr	core region
ch	channel
cs	cross-section
e	equivalent
f	fluid
h	hydraulic
w	wall
m	mean value
avg	average
out	outlet
in	inlet
1	inner
2	outer

Abbreviations

ICT	internally channeled tube

1. Introduction

A growing demand on energy sustainability has led to the need for more compact and efficient heat exchangers [1]. Among various methods for improving thermal efficiency of heat exchangers, passive techniques are widely employed. They include extending the heat transfer area or inducing turbulence in fluid flow to reduce thermal resistance [2,3]. Several techniques involving the use of finned, corrugated, or helical tubes, can enlarge the heat transfer area [2]. Investigations presented in Refs. [4–6] examined the utilization of streamwise or wavy fins and corrugated surfaces within the annulus region of a double-pipe heat exchanger. It was found that increasing the fin size or elevating the corrugation height in the annulus region results in a larger heat transfer area, thereby improving heat transfer efficiency. Another method to intensify the turbulence in the fluid flow and simultaneously to increase heat transfer area is based on twisted geometries, such as twisted tape inserts within cylindrical tubes or incorporated V-winglets on the tube surface [7–9]. The latter method was demonstrated in several publications (e.g., Refs. [10–12]) as an effective means of improving thermal performance.

However, with the most available passive techniques used to optimize heat exchangers, improvement could be achieved only within either a cold or a hot fluid. Furthermore, the techniques targeting enlarged heat transfer area between the two fluids in contact hardly bring about a significant enlargement. In contrast, the internally channeled tube (ICT) concept provides a significantly better possibility based on the use of specifically designed curved channels placed within a circular tube along its length. This design allows for a significant increase in the heat transfer area between two fluids in contact, leading to a substantial enhancement in the thermal performance.

The ICT concept was introduced and investigated, both numerically and experimentally, in the previous studies [13,14]. Basically, ICT consists of two flow regions, the core and the channels, that are arranged along the insulated outer wall of the tube (see Fig. 1a). A hot fluid is assumed to flow along the core region of the tube, while a cold fluid flows counter-currently along the channels. In this way, the loss of heat into the surroundings can be reduced and ultimately less insulation material is needed. The geometry of ICT was determined based on the inner and outer curves defined by Eq. (1) and illustrated in Fig. 1b

$$x = f(y)_i = f(y)_o = c + 81 \cdot \delta \cdot \left(\frac{y}{\delta}\right)^{\alpha_1} - 32 \cdot \Gamma \cdot \left(\frac{y}{\Gamma}\right)^{\alpha_2} \tag{1}$$

The indices *i* and *o* denote the application of Eq. (1) either to the inner or to the outer curve. The values of the coefficients δ and Γ and exponents α_1, and α_2 can be found in Ref. [13].

The ICT heat exchanger performance was evaluated in comparison to the reference "double pipe heat exchanger" (DPHE) under specific constraints. The comparison revealed a remarkable heat transfer rate enhancement of ICT up to 50 % under turbulent flow

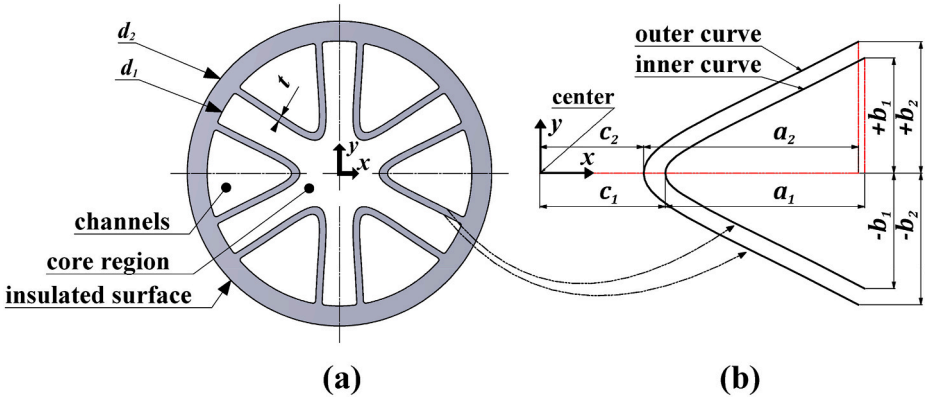

Fig. 1. Cross-sectional view of the ICT (**a**); ICT inner and outer curves together with geometrical parameters a_m, b_m, and c_m (m:1,2) (**b**).

conditions [13]. Furthermore, the Performance Evaluation Criterion (PEC) was used to account for the consumed pumping power, which includes both the gained heat transfer rate and pressure loss. PEC was found to be greater than one, indicating that the improvement in heat transfer within ICT prevails over the associated increase in pressure drop [13].

Reliable design methods for ICT are necessary. However, correlations for pressure drop and heat transfer coefficients governing turbulent flows in non-circular ducts are very scarce. Available non-circular correlations are primarily designed for specific cross-sectional geometries, which may not be directly applicable to ICT duct geometries. This was the reason to utilize established correlations for circular geometries (cf. Ref. [13]). Such correlations are widely used for both circular and non-circular tubes, while a certain adjustment of the Reynolds numbers, namely a replacement of a circular tube diameter by a corresponding hydraulic diameter of a non-circular tube, is applied. The hydraulic diameter is defined as four times the cross-sectional area of the duct divided by its wetted perimeter.

The correlations explored in Ref. [13] were suggested by Gnielinski [15], Nikuradse [16], and Drew and MacAdams [17] for the friction factor and by Gnielinski [15], Dittus and Boelter [18], and Petukhov [19], for the Nusselt number. These established correlations served as a means to qualitatively evaluate the feasibility of the CFD model in the absence of experimental validation. A more sound experimental validation was performed in a later work [14].

The need for new correlations for ICT that duly account for their specific, non-circular geometry and cover realistic flow and boundary conditions remains. One of the essential reasons is the presence of insulated outer surface in ICT, which makes the direct application of existing published correlations to ICT ducts unfeasible. It is why in Ref. [13], a special adjustment was made for the Nusselt number correlations from Refs. [15,18,19]. The adjustment was deemed necessary due to a difference between the length scale used in these correlations and the appropriate length scale for calculating the Nusselt number for ICT ducts. The adjusted correlations were applied in Ref. [13] to two specific ICT geometries, and their performance was reasonably good. However, this cannot be guaranteed for further ICT modifications toward their optimization, for instance when the duct shape or the number of channels change. To cover a wider range of geometrical parameters and avoid significant inaccuracy, appropriate novel correlations must be developed.

In this work, such correlations were derived for the thermohydraulic design of ICT under turbulent forced convection and countercurrent flow conditions. The correlations were developed based on the results obtained by the CFD simulations in Ref. [13] complemented by additional numerical data generated in this work. Preliminary sensitivity studies were carried out, both for the friction factor and for the Nusselt number, to identify geometrical parameters of ICT ducts with high impact. This helped to integrate the most influential parameters into the developed correlations thus improving their predictivity.

2. CFD modelling and boundary conditions

In Ref. [13], comprehensive CFD simulations of turbulent and laminar forced convection heat transfer in ICTs were presented for two different geometrical configurations of ICT. The heat transfer was modeled using a conjugate formulation. Velocity, pressure, and temperature fields were determined numerically by solving three-dimensional continuity, momentum, and energy equations, based on the finite volume method (FVM). The CFD simulations were carried out on a cluster at the Paderborn Center for Parallel Computing (PC^2) using Ansys Fluent software. The realizable k-ϵ model [20] was applied to govern Reynolds stresses in a turbulent single-phase flow. The realizable k-ϵ model offers several benefits including a good performance in round jets with complex flow characteristics, fast convergence, low computation costs, and successful application to complex unit geometries [21]. In Ref. [13], the turbulent flow in the ducts of ICT design shown in Fig. 1a was studied for the Reynolds numbers ranges $10000 \leq Re_h \leq 30000$ in the core region and $3000 \leq Re_h \leq 8600$ in the channels. A successful validation against experimental data followed in Ref. [14].

The computational domain comprised two fluid regions separated by a wall and bounded by symmetrical planes set at a 60° angle. The total length of the domain is 1 m for both the core region and the channel. Conjugate boundary conditions were adopted at fluid-wall interfaces to ensure the heat flux continuity across the inner wall. Zero-gradient boundary conditions for velocity components and temperature were applied at symmetry planes while a no-slip condition was used at the wall. On the outer-tube wall, an adiabatic

boundary condition was employed since ICT is insulated from the outer surface. As inlet boundary conditions, fully developed velocity profiles and constant temperatures were utilized. At the outlet boundaries of the core region and of the channel, zero static pressure was set for the momentum equation, and a zero-gradient temperature condition was applied for the energy equation.

3. Process parameters

In the CFD analysis carried out in Ref. [13], it was assumed that the flows in the adjacent horizontally oriented channels of the ICTs were incompressible, single-phase, counter-current, steady-state, and with constant fluid properties.

The Reynolds number of the flow in the ICT is defined based on the hydraulic diameter:

$$\mathrm{Re}_h = \frac{u_m\, D_h}{\nu} \tag{2}$$

Here, u_m is the mean velocity:

$$u_m = \frac{\dot{m}}{\rho\, A_{cs}} \tag{3}$$

and D_h is the hydraulic diameter:

$$D_h = \frac{4A_{cs}}{P_h} \tag{4}$$

with P_h being the wetted perimeter and A_{cs} the cross-sectional area of a duct.

The channel cross-sectional area (A_{ch}) of ICT is determined by numerical integration according to Eq. (5) using Eq. (1) for the inner curve within the known domain ($-b \le y \le +b$).

$$A_{ch} = \int_{-b}^{+b} \left[\left(\sqrt{\left(d_1/2 \right)^2 - y^2} \right) - f(y)_i \right] dy \tag{5}$$

The cross-sectional area of the core-region (A_{cr}) can be calculated by subtracting the total area enclosed by the outer curves from the area of the inner pipe as follows:

$$A_{cr} = \left(\pi {d_1}^2/4 \right) - 6 \cdot Area_{under\ outer\ curve} \tag{6}$$

The area under the outer curve is determined by:

$$A_{under\ outer\ curve} = \int_{-b}^{+b} \left[\left(\sqrt{\left(d_1/2 \right)^2 - y^2} \right) - f(y)_o \right] dy \tag{7}$$

The friction factor is expressed by:

$$f = \frac{D_h\, \Delta p}{2\, \rho\, {u_m}^2 l} \tag{8}$$

where Δp is the difference between the pressure values at the inlet and outlet boundaries.

Nusselt number based on equivalent diameter (D_e) is defined as follows:

$$\mathrm{Nu}_e = \frac{h_{avg} \cdot D_e}{\lambda_f} \tag{9}$$

where h_{avg} represents the surface-average heat transfer coefficient:

$$h_{avg} = \frac{q}{T_W - T_b} \tag{10}$$

Here, q is heat flux per unit area [W/m^2] in the direction normal to the inner wall, T_W is the mean wall temperature determined as the surface average temperature of the interface between the fluid and the solid wall, and T_b is the mean bulk temperature. The latter was calculated by averaging over the cross-sections, either in the core region or in the channel, as follows:

$$T_b = \frac{\int_{A_{cs}} uTdA}{\int_{A_{cs}} udA} \tag{11}$$

This integration was performed for the five consecutive cross-sections along the test section for the respective flows.

The equivalent diameter (D_e) in Eq. (9) is determined by the equivalent perimeter (P_e), over which heat transfer takes place:

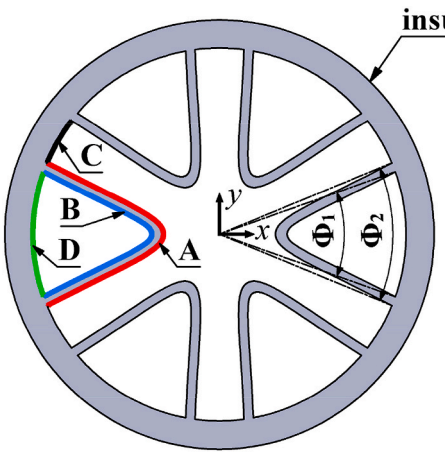

Total perimeter		perimeter type
core region	channel	
6 · (A+C)	B+D	hydraulic
6 · A	B	equivalent

Fig. 2. Illustration of equivalent and hydraulic perimeters of ICT for the core region and channels.

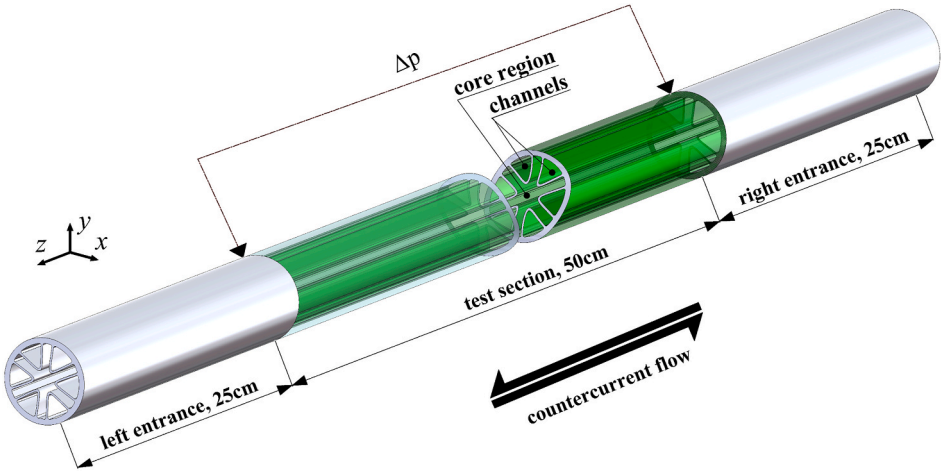

Fig. 3. A schematic of an ICT heat exchanger.

$$D_e = \frac{4A_{cs}}{P_e} \tag{12}$$

As a result of the insulation of the ICT outer surface, there is no heat transfer through this surface and only the inner wall represented by the equivalent perimeter is responsible for heat transfer (cf. Fig. 2). Therefore, the calculation of the equivalent diameter is only based on the perimeter of the fluid faces involved in heat transfer [22]. This leads to the absence of thermal boundary layers on the insulated walls, in contrast to the formation of such hydrodynamic boundary layers everywhere near the duct walls [13]. The equivalent (P_e) and hydraulic (P_h) perimeters in the cross-sections of the core regions and channels are illustrated in Fig. 2. The equivalent perimeters shown in red and light blue curves represent the area between the hot and cold fluids, which is calculated using Eq. (13). The length of the insulated perimeters is represented by the black and green curves, determined by Eqs. (14) and (15). The table in Fig. 2 provides a detailed explanation of the lengths of the hydraulic and equivalent perimeters.

$$Arc\ length(perimeter) = \int_{-b}^{+b} \sqrt{1 + \left(f'(y)_{i,o}\right)^2}\, dy \tag{13}$$

$$Arc\ length_{\ D} = (d_1/2) \cdot \Phi_1 \cdot (\pi/180) \tag{14}$$

$$Arc\ length_{\ C} = (\pi d_1/6) - [(d_1/2) \cdot \Phi_2 \cdot (\pi/180)] \tag{15}$$

4. Validation of the CFD-based model

In [14], the results of the experimental study of ICT designs were published. The measured pressure drop and temperatures were used to validate the model developed in Ref. [13]. In both experimental and numerical studies [13,14], pressure drop and heat transfer coefficient were evaluated for the middle part of ICT (the test section). Moreover, the dimensions of the investigated ICT design were selected based on experimental needs, allowing for ease of manufacturing and a convenient setup in a laboratory environment. The

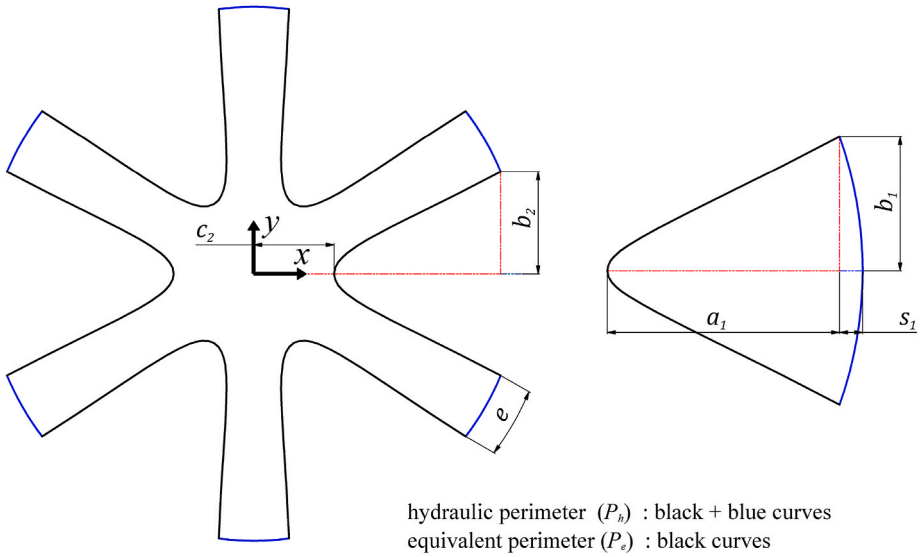

Fig. 4. Cross-section of ICT ducts with characteristic geometries: core region (left); channel (right).

inner (d_1) and outer (d_2) diameters of the tubes (shown in Fig. 1) are 40 mm and 46 mm, respectively. The internal wall thickness (t) of the channels is 1 mm, and the total length of ICT is 1 m.

The numerical and experimental results agree well over the entire studied Reynold number range ($2500 \leq \mathrm{Re}_h \leq 18000$). The maximum deviation for pressure drop was below 6.5 %, for both core region and channel flow. Also, the heat transfer coefficients determined by simulations and by measurements were in good agreement with a maximum deviation of 13 % [14].

5. Design equations for friction factor

Pressure drop in the core region and channels of ICT is primarily caused by fluid-wall friction. Pressure drop was evaluated only within the middle section of 50 cm (test section), by excluding the entrances (cf. [13,14]), and it is determined as the difference between the pressure values at the inlet and outlet of the middle section (cf. Fig. 3). In the turbulent flow, the entrance length is typically short, approximately 10–20 times the hydraulic diameter [23]. Applying this evaluation to ICT ducts, it approximately results in an entrance length of less than 25 cm. This can ensure stabilized flow in the mid-section (test section) of the ICT. Due to the horizontal orientation, gravitational effects are neglected. The Fanning friction factor is obtained by Eq. (8).

The power law function ($f = mRe^j$, where m and j are constants) is commonly used to estimate friction factors in circular ducts [24]. It is a straightforward approach to incorporate the substantial influence of the Reynolds number. However, in non-circular ducts, the friction factor can also be influenced by duct geometry [25,26]. In a number of studies, friction factors or Nusselt numbers in non-circular passages were correlated by employing geometrical parameters. Duan et al. [27,28] developed correlations to predict pressure drop in arbitrary-shape ducts based on the aspect ratio, defined as the minor axis to the major axis of the duct. It was found that duct cross-sections may have a significant influence on the friction factor. Piper et al. [29] presented correlations to govern pressure loss in the turbulent flow within the inner channel of a pillow-plate heat exchanger; the correlations contain geometrical parameters of the channel.

It is, therefore, necessary to establish correlations for ICT ducts, with due considerations of geometrical parameters (e.g., a_1, b_1, b_2, c_2), so that ICT can be designed and optimized accordingly. The geometrical parameters a_1, b_1, b_2, c_2, s_1, P_h and e shown in Fig. 4 were identified in this study as having an impact on friction factor in the ICT ducts. The influence of the characteristic geometrical parameters on the friction factor was analyzed using the CFD simulations performed in Ref. [13]. Additional numerical data was generated in this work in a similar way as in [13]. This helped to extend the correlations applicability. Dimensionless parameter combinations can be built in relation to the inner radius of the tube as follows:

$$\vartheta = (a_1 + s_1)/r \tag{16}$$

$$\eta = 2b_1/r \tag{17}$$

$$\gamma = 2b_2/r \tag{18}$$

$$\psi = c_2/r \tag{19}$$

$$\varphi = e/r \tag{20}$$

$$\beta_h = P_h/r \tag{21}$$

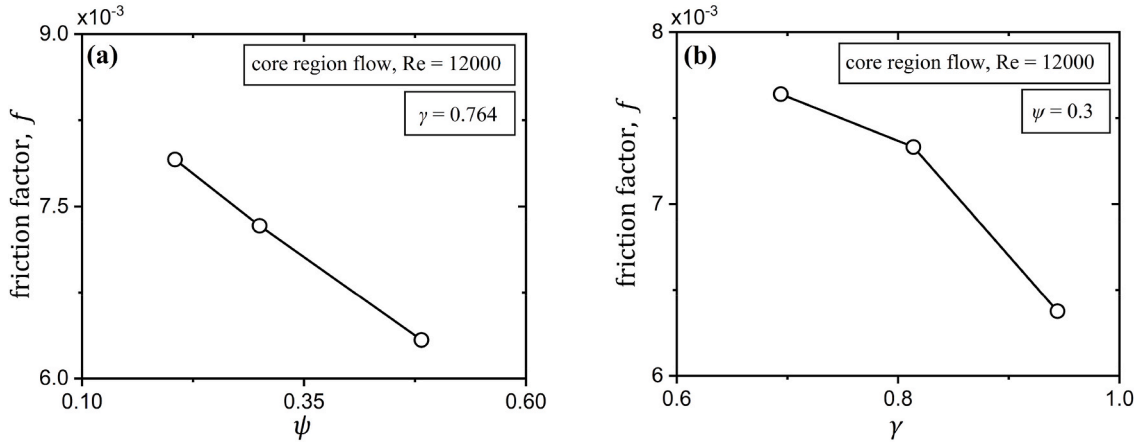

Fig. 5. The influence of the dimensionless geometrical parameters ψ (**a**) and γ (**b**) on the Fanning friction factor in the **core region** of ICT.

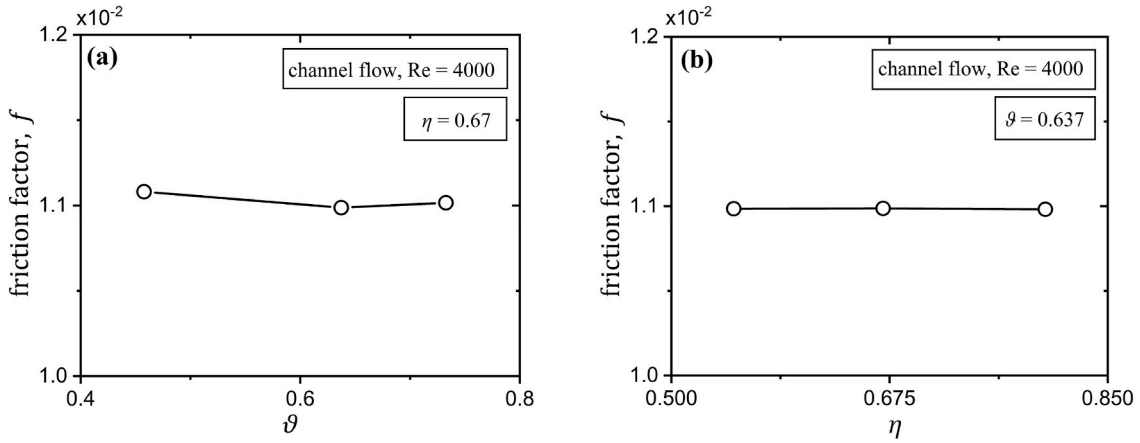

Fig. 6. The influence of the dimensionless geometrical parameters ϑ (**a**) and η (**b**) on the Fanning friction factor in the **channel** region of ICT.

Table 1
Summary of coefficients of Eqs. (22) and (23) and geometrical parameter ranges for the friction factor.

	core region flow			channel flow	
	$f = n_1\,\mathrm{Re}_h^{n_2}(\gamma)^{n_3-\varphi}(\beta_h)^{n_4}$			$f = n_5\,\mathrm{Re}_h^{n_6}(\beta_h)^{n_7}$	
	$0.5 \le \gamma \le 1,\ 8 \le \beta_h \le 13,\ 0 \le \varphi \le 0.4$			$0.5 \le \eta \le 1,\ 1.7 \le \beta_h \le 2.6$	
	$0.2 \le \psi \le 0.32$	$0.34 \le \psi \le 0.5$		$0.35 \le \vartheta \le 0.56$	$0.58 \le \vartheta \le 0.70$
n_1	0.0414	0.1650	n_5	0.2535	0.240
n_2	−0.3175	−0.3040	n_6	−0.3436	−0.360
n_3	0.1400	0.2250	n_7	−0.4580	−0.128
n_4	0.5190	−0.1570			

Here r is a half of the inner diameter (d_1) (cf. Figs. 1 and 4).

The influence of characteristic geometry parameters on the Fanning friction factor in ICT ducts is demonstrated in Figs. 5 and 6. Fig. 5 reveals a substantial impact of the parameters ψ and γ at $\mathrm{Re}_h = 1200$ on the friction factor. In contrast, the geometrical parameters have nearly no influence in the channel region, as can be seen in Fig. 6, which shows the results for the varied ϑ at a constant values of $\eta = 0.67$ (Fig. 6a) and for the varied η at $\vartheta = 0.637$ (Fig. 6b), at $\mathrm{Re}_h = 4000$.

The following correlations are proposed for the friction factor for single-phase flow:

for the core region:

$$f_{cr} = n_1 \mathrm{Re}_h^{n_2}\,(\gamma)^{n_3-\varphi}(\beta_h)^{n_4} \tag{22}$$

for the channels:

$$f_{ch} = n_5\,\mathrm{Re}_h^{n_6}\,(\beta_h)^{n_7} \tag{23}$$

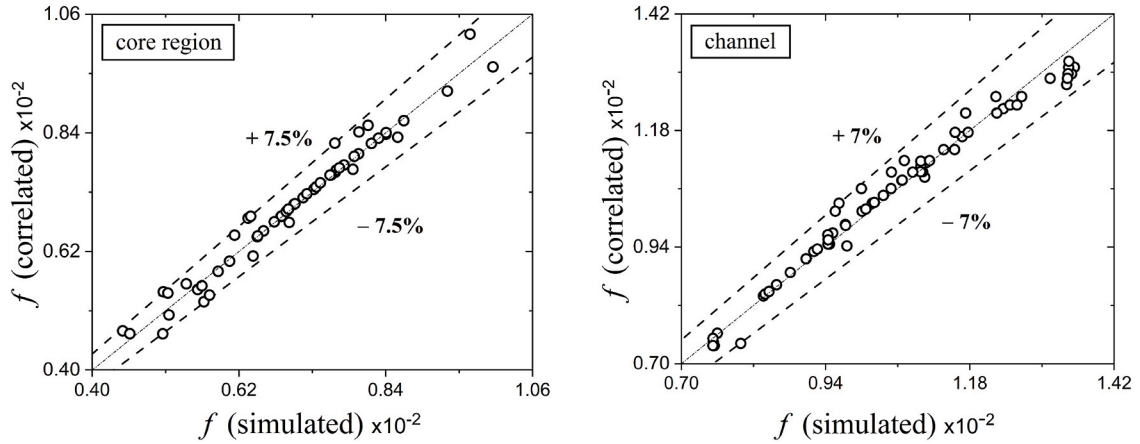

Fig. 7. Comparison between friction factors obtained by simulations in Ref. [13] and in this study and those calculated by Eq. (22) (left) and Eq. (23) (right) with coefficients from Table 1.

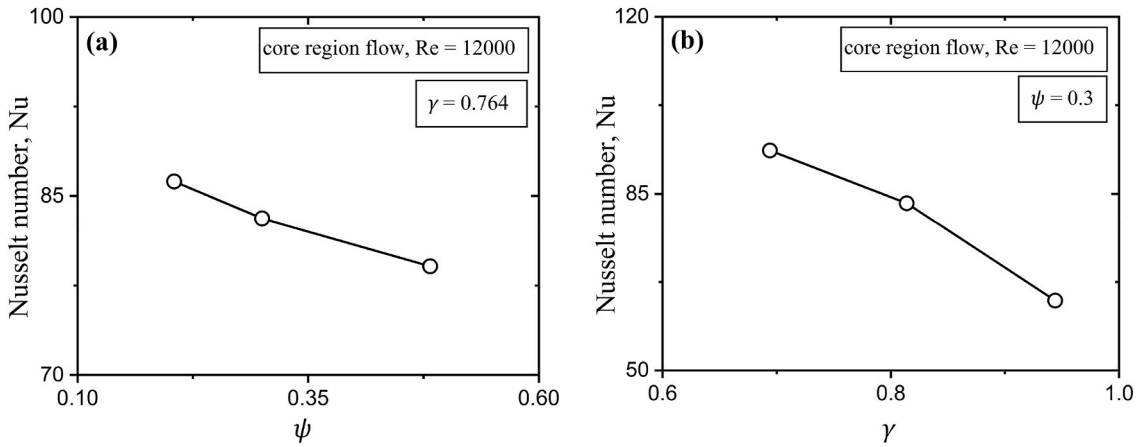

Fig. 8. The influence of the dimensionless geometrical parameters: ψ (**a**); and γ (**b**) on the Nusselt number in the **core region** of ICT.

Here n_1 to n_7 are the coefficients of the correlations to be determined by nonlinear regression analysis. This well-known numerical method uses input values (Reynolds numbers and geometrical parameters of ICT ducts) and fitting correlations, Eqs. (22) and (23); their results are compared with the values obtained by CFD simulations. Minimization of the residual sum of squares (RSS) yields the values n_1 to n_7. The obtained coefficients of Eqs. (22) and (23) are presented in Table 1. The CFD data used in this analysis is based on the pressure drop values extracted from CFD simulations published in Ref. [13] and performed in this work.

According to the trend discussed above (cf. Fig. 6), the dimensionless combination η is omitted in Eq. (23). The ratio β_h of the hydraulic perimeter to the radius is included in both correlations to obtain accurate predictions for various geometries. This inclusion helps to capture the impact of the complex wall curvature more precisely, as this cannot be done properly using the parameters a, b, c only. Moreover, Eq. (22), contains an additional exponent φ, which represents the ratio of the peripheral distance between every two channels in the core region to the inner radius, $\varphi = e/r$. The parameters β_h and φ were found to have a similar impact on friction factor as the parameters ψ and γ (cf. Fig. 5). The variation ranges of the geometrical parameters studied in this work are summarized in Table 1.

The developed correlations, Eqs. (22), (23), are compared with the CFD results in Fig. 7. With the proposed equations, the Fanning friction factor in ICT ducts can be reproduced with good accuracy, with the maximum deviation being 7.5 % for the core region and 7 % for the channel flow. Nearly 95 % of the data falls within a maximum deviation of less than 5 %. The validity range for the Reynolds number is $6000 \leq \mathrm{Re}_h \leq 40000$ for core region flow and $2500 \leq \mathrm{Re}_h \leq 15000$ for channel flow.

6. Design equations for Nusselt number

Commonly, the Nusselt number correlations are represented in a simple form of Dittus-Boelter [18] which is a power-law equation. This form is used for turbulent flows in smooth pipes and describes the dependence of the Nusselt number on the Reynolds and Prandtl numbers. However, this equation form may not sufficiently capture the Nusselt number behavior for complex geometries found in

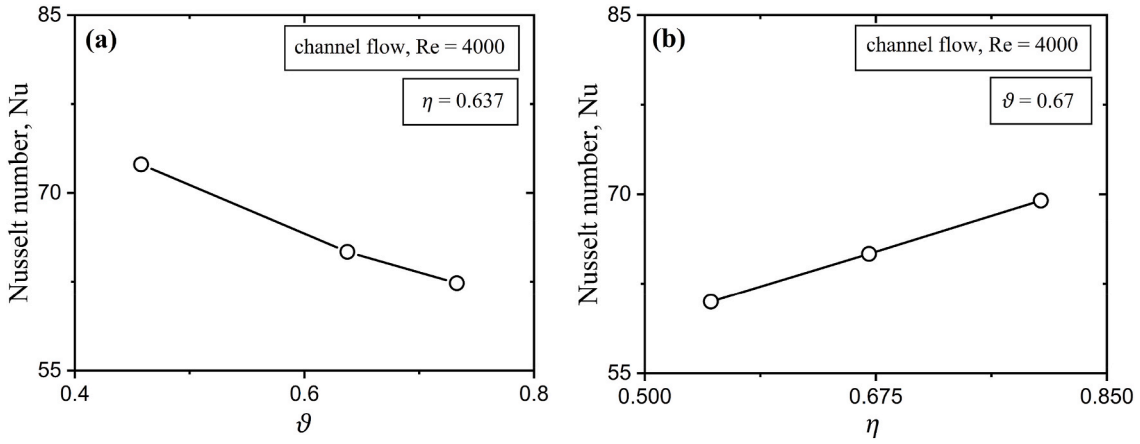

Fig. 9. The influence of the dimensionless geometrical parameters: ϑ (**a**); and η (**b**) on the Nusselt number in the **channel** of ICT.

Table 2
Summary of coefficients of Eqs. (24) and (25) and geometrical parameter ranges for the Nusselt number.

	core region flow			channel flow	
	$\mathrm{Nu} = m_1\,\mathrm{Re}_h^{m_2}(\gamma)^{m_3-\varphi}(\beta_e)^{m_4}\,\mathrm{Pr}^{0.3}$			$\mathrm{Nu} = m_5\,\mathrm{Re}_h^{m_6}(\eta)^{m_7}(\beta_e)^{m_8}\,\mathrm{Pr}^{0.4}$	
	$0.5 \le \gamma \le 1,\ 7 \le \beta_e \le 12,\ 0 \le \varphi \le 0.40$			$0.5 \le \eta \le 1,\ 1 \le \beta_e \le 1.6$	
	$0.2 \le \psi \le 0.35$	$0.38 \le \psi \le 0.50$		$0.35 \le \vartheta \le 0.56$	$0.58 \le \vartheta \le 0.70$
m_1	0.0695	0.166	m_5	0.0400	0.020
m_2	0.8120	0.811	m_6	0.8025	0.872
m_3	−0.0460	−1.120	m_7	0.5180	0.175
m_4	−0.4550	−1.010	m_8	0.2480	0.180

non-circular ducts [30,31]. The complex shape of non-circular ducts has a direct impact on the velocity and temperature distributions. This results in a particular fluid flow and heat transfer behavior, which differs from what can be typically observed in circular ducts [32]. Thus, a straightforward application of the Dittus-Boelter [18] correlation to non-circular ducts is hardly possible; rather, it has to be modified and adapted by incorporating relevant geometric parameters of the specific non-circular duct.

In this study, numerical analysis was performed to examine the impact of geometrical parameters shown in Fig. 4 on the Nusselt number. This analysis was carried out in a similar way as for the friction factor (cf. Section 5), and the geometrical parameters were subsequently incorporated into the power-law form of the Dittus-Boelter [18]. In Figs. 8 and 9, the dependence of the Nusselt number on different combinations of the ICT geometrical parameters is demonstrated. The qualitative trends shown on Fig. 8 for the core region flow are similar to those visible on Fig. 5. This similarity does not hold for the dependencies of the Nusselt number on geometrical parameters ϑ and η at $\mathrm{Re}_h = 4000$ (cf. Fig. 9). It is clearly seen that the geometrical parameters of ICT ducts have a substantial impact on the Nusselt number.

For single-phase fully developed flows, the following new correlations for the Nusselt number are proposed:

for the core region:

$$Nu_{cr} = m_1 \mathrm{Re}_h^{m_2}\,(\gamma)^{m_3-\varphi}(\beta_e)^{m_4}\,\mathrm{Pr}^{0.3} \tag{24}$$

for the channel:

$$Nu_{ch} = m_5\,\mathrm{Re}_h^{m_6}(\eta)^{m_7}(\beta_e)^{m_8}\,\mathrm{Pr}^{0.4} \tag{25}$$

Here m_1 to m_8 are the coefficients evaluated by the regression analysis in a similar way as described in Section 5. This evaluation was performed based on the heat transfer coefficients obtained from the detailed CFD simulations performed both previously [13] and in this study. The obtained coefficients (m_1 to m_8) are presented in Table 2.

It should be mentioned that the Nusselt number correlations represented by Eqs. (24) and (25) contain a different geometrical parameter than the correlations for the friction factor (Eq. (22), (23)). The latter utilize the hydraulic perimeter, while Eqs. (24) and (25) use the equivalent perimeter (P_e) defined as follows:

$$\beta_e = P_e / r \tag{26}$$

Calculation of the equivalent diameter (12) is based only on the perimeter of the fluid faces taking part in heat transfer (cf. Section 3). In Eqs. (24) and (25), Prandtl number exponents are kept as specified in the formulation given by Dittus-Boelter [18] for the cold side (0.4) and for the hot side (0.3). For water used as a working fluid in our previous and present investigations, Prandtl number range is limited to $2 \le \mathrm{Pr} \le 10$.

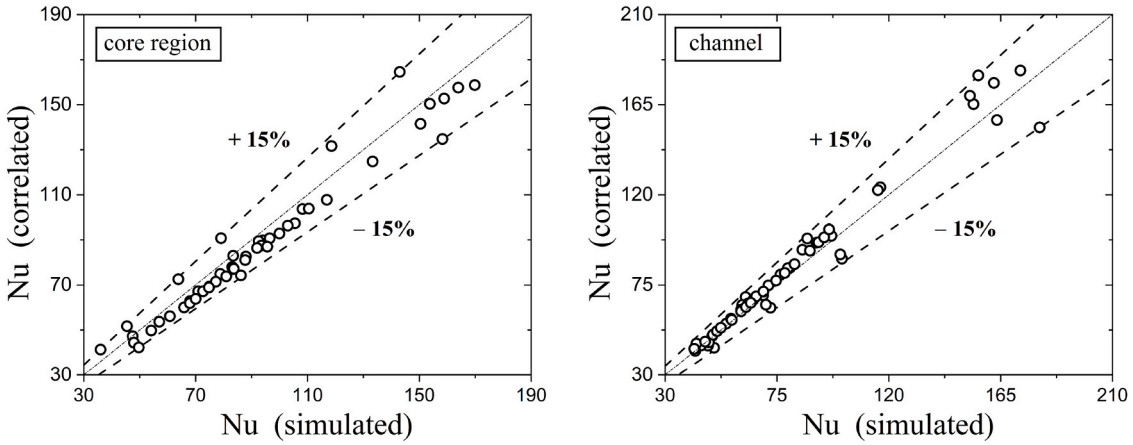

Fig. 10. Comparison between Nusselt number obtained by simulations in Ref. [13] and in this study and those calculated by Eq. (24) (left) and (25) (right) with coefficients from Table 2.

Fig. 10 shows a comparison of Nusselt number values for ICT ducts obtained by the CFD results and by the developed correlations, Eqs. (24) and (25). The simulated Nusselt numbers are accurately reproduced, with a maximum deviation of ±15 % for both the core region and channel of ICT, while nearly 95 % of the data show deviations less than 10 %. The validity range for the Reynolds number is $2500 \leq Re_h \leq 15000$ for channel flow and $6000 \leq Re_h \leq 40000$ for core region flow, while the Prandtl number is varied between 2 and 10.

7. Conclusions

The internally channeled tube (ICT) concept represents a promising heat exchanger design with superior thermal performance. However, lacking design methods hinder its practical application. Because of non-circular geometry of ICT and the presence of an insulated outer surface, its rigorous description under typically complex flow conditions presents a considerable challenge. Consequently, the focus of this study is to develop new correlations describing pressure drop and heat transfer characteristics in the ICT designs for turbulent forced convection.

The correlations were derived from the results of extensive CFD simulations obtained with the previously developed tool [13]. The underlying model was validated for turbulent flow conditions in Ref. [14]. A sensitivity analysis of the CFD results was carried out to find relevant geometrical parameters of the ICT ducts to be included in the correlations for the friction factor and Nusselt number. The developed correlations show maximum deviations of 7.5 % from the numerical results for the friction factor; for the Nusselt number, this value is 15 %. The correlations are valid for a broad range of ICT geometrical parameters and Reynolds numbers. Future studies are devoted to the extension of the ICT heat exchanger description to cover laminar flow conditions.

CRediT authorship contribution statement

Abbas J.S. Al-Lami: Conceptualization, Data curation, Investigation, Methodology, Software, Validation, Writing – original draft. **Eugeny Y. Kenig:** Resources, Supervision, Writing – review & editing.

Declaration of competing interest

The authors declare that they have no known competing financial interests or personal relationships that could have appeared to influence the work reported in this paper.

Data availability

No data was used for the research described in the article.

Acknowledgements

Abbas Al-Lami is grateful for the financial support provided by the German Academic Exchange Service DAAD (award number 91725535). The authors also gratefully acknowledge the funding of this project by computing time provided by the Paderborn Center for Parallel Computing (PC^2). Furthermore, the authors appreciate the publication cost coverage by the Open Access Publication Fund of Paderborn University.

References

[1] N.H. Afgan, M. da Graça Carvalho, Sustainability assessment of heat exchanger design, in: Sustainable Assessment Method for Energy Systems, Springer, Boston, MA, 2000, pp. 127–138, https://doi.org/10.1007/978-1-4615-4479-1_6.

[2] M.H. Mousa, N. Miljkovic, K. Nawaz, Review of heat transfer enhancement techniques for single phase flows, Renew. Sustain. Energy Rev. 137 (2021) 110566, https://doi.org/10.1016/J.RSER.2020.110566.

[3] L. Liebenberg, J.P. Meyer, In-tube passive heat transfer enhancement in the process industry, Appl. Therm. Eng. 27 (2007) 2713–2726, https://doi.org/10.1016/j.applthermaleng.2007.06.003.

[4] T. Ma, M. Lin, M. Zeng, Y.P. Ji, Q.W. Wang, Numerical study of internally finned bayonet tubes in a high temperature bayonet tube heat exchanger with inner and outer fins, Proc. ASME Turbo. Expo. 5 (2010) 329–338, https://doi.org/10.1115/GT2010-22360.

[5] Q.W. Wang, M. Lin, M. Zeng, L. Tian, Investigation of turbulent flow and heat transfer in periodic wavy channel of internally finned tube with blocked core tube, J. Heat Transf. 130 (2008) 1–7, https://doi.org/10.1115/1.2891219.

[6] X. Liu, M.K. Jensen, Geometry effects on turbulent flow and heat transfer in internally finned tubes, J. Heat Transf. 123 (2001) 1035–1044, https://doi.org/10.1115/1.1409267.

[7] Z. Azizi, V. Rostampour, S. Jafarmadar, S. Khorasani, B. Abdzadeh, Performance evaluation of horizontal straight tube equipped with twisted tape turbulator, with air–water two-phase flow as working fluid, J. Therm. Anal. Calorim. 147 (2022) 4339–4353, https://doi.org/10.1007/s10973-021-10809-z.

[8] R. Rezazadeh, S. Jafarmadar, S. Khorasani, S.R.A. Niaki, Experimental investigation on thermal behavior of non-boiling slug and bubbly two phase-flow in helical tube with spiral, J. Mech. Eng. Sci. 236 (2022) 3434–3446, https://doi.org/10.1177/09544062211042045.

[9] R.A. Rezaei, S. Jafarmadar, S. Khorasani, Presentation of frictional behavior of micro helical tubes with various geometries and related empirical correlation; an experimental study, Int. J. Therm. Sci. 140 (2019) 377–387, https://doi.org/10.1016/j.ijthermalsci.2019.03.011.

[10] P. Promvonge, S. Skullong, Enhanced thermal performance in tubular heat exchanger contained with V-shaped baffles, Appl. Therm. Eng. 185 (2021), https://doi.org/10.1016/j.applthermaleng.2020.116307.

[11] P. Promvonge, P. Promthaisong, S. Skullong, Thermal performance augmentation in round tube with louvered V-winglet vortex generator, Int. J. Heat Mass Transf. 182 (2022), https://doi.org/10.1016/j.ijheatmasstransfer.2021.121913.

[12] X. Wu, T. Fu, J. Wang, L. Zeng, F. Zhang, A comparative study of fluid flow and heat transfer in the tube with multi-V-winglets vortex generators, Appl. Therm. Eng. 236 (2024), https://doi.org/10.1016/j.applthermaleng.2023.121448.

[13] A.J.S. Al-Lami, V. Inguva, E.Y. Kenig, Numerical analysis of conjugate heat transfer within internally channeled tubes, Appl. Therm. Eng. 223 (2023) 119596, https://doi.org/10.1016/j.applthermaleng.2022.119596.

[14] A.J.S. Al-Lami, Eugeny Y. Kenig, Experimental study of an internally channeled tube heat exchanger under turbulent flow conditions, Int. J. Heat Mass Transf. 214 (2023) 124425, https://doi.org/10.1016/j.ijheatmasstransfer.2023.124425.

[15] V. Gnielinski, New equations for heat and mass transfer in turbulent pipe and channel flow, Int. Chem. Eng. 16 (1976) 359–368.

[16] J. Nikuradse, Laws of Flow in Rough Pipes, NACA, Washington, 1950.

[17] T.B. Drew, W.H. McAdams, The friction factor for clean round pipe, AIChE 28 (1932) 56–72.

[18] F.W. Dittus, L.M.K. Boelter, Heat transfer in automobile radiators of the tubular type, Int. Commun. Heat Mass Transf. 12 (1985) 3–22, https://doi.org/10.1016/0735-1933(85)90003-X.

[19] B.S. Petukhov, Heat transfer and friction in turbulent pipe flow with variable physical properties, Adv. Heat Transf. 6 (1970) 503–564, https://doi.org/10.1016/S0065-2717(08)70153-9.

[20] T.H. Shih, W.W. Liou, A. Shabbir, Z. Yang, J. Zhu, A new k-ϵ eddy viscosity model for high Reynolds number turbulent flows, Comput. Fluids 24 (1995) 227–238, https://doi.org/10.1016/0045-7930(94)00032-T.

[21] P.A. Davidson, Turbulence: an Introduction for Scientists and Engineers, 2nd ed., Oxford University Press, 2004.

[22] J.P. Duarte, M.L. Corradini, Hydraulic and heated equivalent diameters used in heat transfer correlations, Nucl. Tech. 201 (2017) 99–102, https://doi.org/10.1080/00295450.2017.1389594.

[23] Y.A. Çengel, J.M. Cimbala. Fluid Mechanics: Fundamentals and Applications, McGraw Hill, 2006.

[24] J. Fiuza Branco, C. Pinho, R. De, A. Figueiredo, From a power-law equation for the friction factor in smooth pipes to a controversy on the overlap layer, in: Proc. 6th International Conference on Energy and Environment Research, 2001. https://www.researchgate.net/publication/281649746.

[25] Y.S. Muzychka, M.M. Yovanovich, Modeling Nusselt numbers for thermally developing laminar flow in non-circular ducts, in: 7th AIAA/ASME Joint Thermophysics and Heat Transfer Conference, 1998, https://doi.org/10.2514/6.1998-2586.

[26] H.C. Claiborne, A Critical Review of the Literature Pressure on Pressure Drop in Noncircular Ducts and Annuli, Oak Ridge, Tennessee, 1952.

[27] Z. Duan, New correlative models for fully developed turbulent heat and mass transfer in circular and noncircular ducts, J. Heat Transf. 134 (2012) 1–6, https://doi.org/10.1115/1.4004855.

[28] Z. Duan, M.M. Yovanovich, Pressure drop for laminar flow in microchannels of arbitrary cross-sections, in: Annual IEEE Semiconductor Thermal Measurement and Management Symposium, IEEE, 2009, pp. 111–120, https://doi.org/10.1109/STHERM.2009.4810751.

[29] M. Piper, A. Zibart, E.Y. Kenig, New design equations for turbulent forced convection heat transfer and pressure loss in pillow-plate channels, Int. J. Therm. Sci. 120 (2017) 459–468, https://doi.org/10.1016/j.ijthermalsci.2017.06.012.

[30] W. Emrich Jr., Thermal fluid aspects of Nuclear rockets, in: Principles of Nuclear Rocket Propulsion, Elsevier, Huntsville, USA, 2016, pp. 117–148, https://doi.org/10.1016/B978-0-12-804474-2.00009-6.

[31] B. Sahin, A Taguchi approach for determination of optimum design parameters for a heat exchanger having circular-cross sectional pin fins, Heat Mass Transf. 43 (2007) 493–502, https://doi.org/10.1007/s00231-006-0224-5.

[32] H. Wang, Z. Chen, J. Gao, Influence of geometric parameters on flow and heat transfer performance of micro-channel heat sinks, Appl. Therm. Eng. 107 (2016) 870–879, https://doi.org/10.1016/j.applthermaleng.2016.07.039.